18th International Conference on Structural Mechanics in Reactor Technology (SMiRT 18)
Beijing, China, August 7-12, 2005
SMiRT18-J02-4

A FATIGUE ASSESSMENT OF PRESSURIZED PIPING ELBOWS WITH LOCAL THINNED AREAS

Cornel Balan
University of Ottawa, Ottawa, Canada
Phone:1-613-562-5800x6370
E-mail: corneliubalan@hotmail.com

Bo Xu
University of Ottawa, Ottawa, Canada
Phone: 1-613-562-5800x6370
Email: boxu261@yahoo.ca

D. Redekop
Department of Mechanical Engineering, University of Ottawa, Ottawa, Canada
Phone:1-613-562-5800x6290, Fax: 1-613-562-5177
E-mail: dredekop@tesla.cc.uottawa.ca

ABSTRACT

An elasto-plastic finite element study was carried out to determine the effect of bi-directional action on the fatigue characteristics of pressurized ninety-degree piping elbows with local thinned areas. Both in-plane and out-of-plane actions were considered to simulate simultaneous horizontal and vertical seismic motions. Two validation studies were conducted, in which present results were compared with previously published results. Studies were then made of eroded piping elbows, i.e. elbows with local thinned areas. A total of 36 models, in six groups, were studied in detail. Variations in the models included positioning of the thinned area, material properties, and magnitude and orientation of the prescribed displacements of the loading. Results were obtained for the deformation and strain patterns, hoop strain histories, and reaction forces. The information provided is useful for qualitative fatigue assessment of elbows using existing fatigue theories.

Keywords: Fatigue; FEM; Elasto-plastic material; Piping elbow; Local thinned area

1. INTRODUCTION

The fatigue analysis problem of eroded piping elbows under seismic action has recently been addressed by a number of authors, including Zhang et al (2001), Shiratori et al (2002), Nakamura et al (2004), and Balan and Redekop (2005). These studies on piping elbows follow work on the performance of straight eroded pipes by Miyazaki et al (2002), and Shim et al (2002), among others, and work on nonlinear-material analysis of undamaged piping elbows by Weisz et al (1996), Mourad and Younan (2001), Tan and Matzen (2002), Mukaimachi et al (2002), Robertson et al (2004), and Kulkarni et al (2004). Important results have been obtained by means of experiments, and by application of the finite element method (FEM).

In this paper the results of an FEM study on the fatigue characteristics of 36 piping elbows are presented. The models are divided into six groups, each containing an undamaged model, and five eroded models. The eroded models have different degrees of thinning. A preliminary validation study serves to verify the current FEM approach. Results are then computed for the six groups of models, determining the influence of the magnitude and direction of the seismic action and of the material properties on the fatigue characteristics.

2. DESCRIPTION OF MODEL AND LOADING

A total of 36 models were studied, divided into six groups. The basic geometry of the models, shown in Fig. 1, followed that of the studies of Shiratori et al (2002) and Balan and Redekop (2005). The elbow had a bend radius of 413 mm, and straight pipes of length 757 mm were attached at either end. The outer diameter of all components was 216.3 mm, and the undamaged thickness was 12.7 mm.

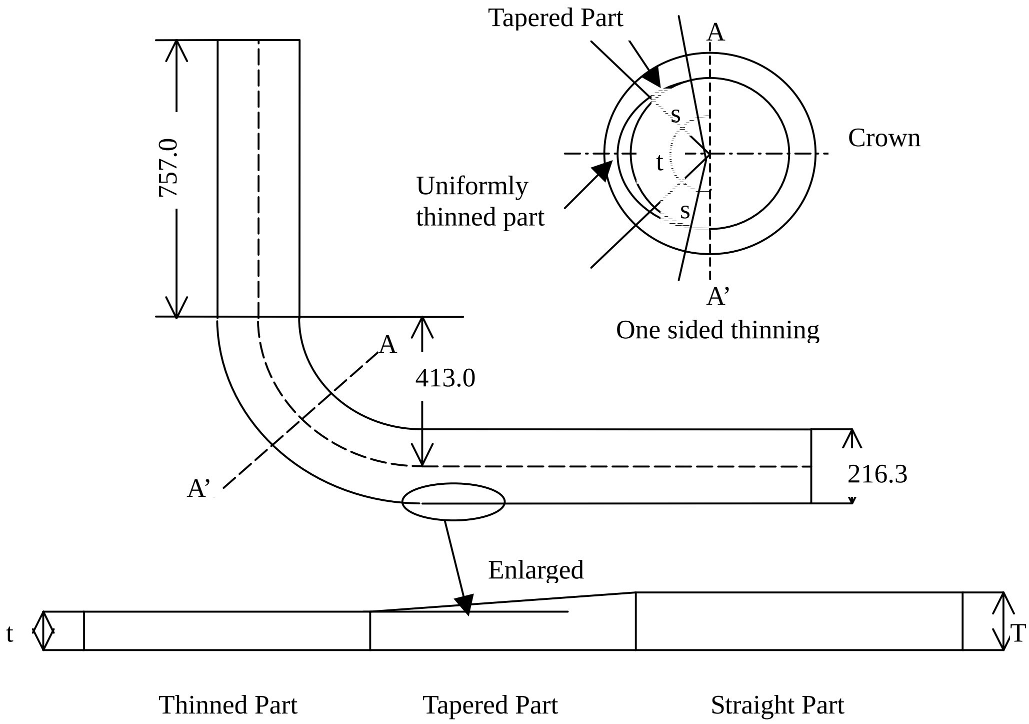

Fig. 1 Details of geometry of piping elbow with local thinned area

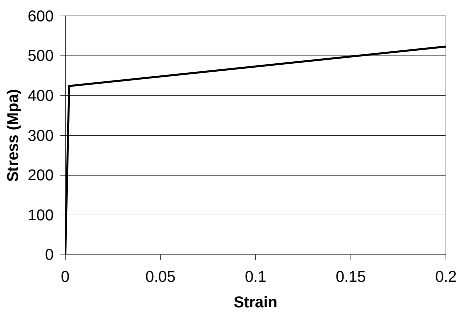

Fig. 2 Material model for STS 410

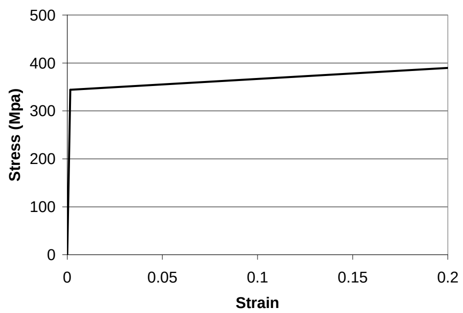

Fig. 3 Material model for SS 304

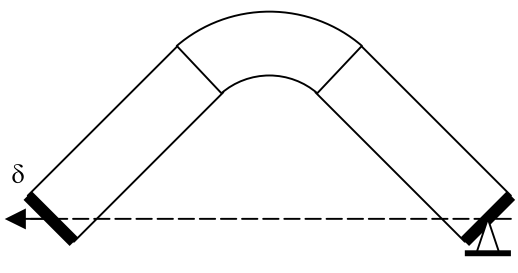

Fig. 4 In-plane prescribed displacement

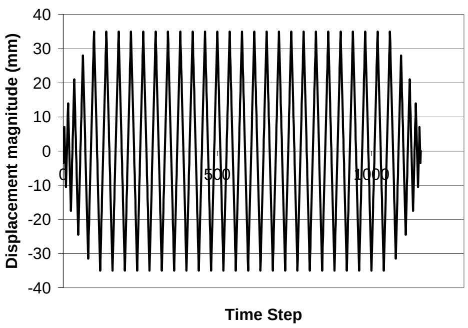

Fig. 5 Displacement δ vs time step

Table 1 Types of thinning

Type	Location	Depth	s (deg)	t (deg)	2s+t (deg)
a	None	0	0	0	0
b	f. c.	50%	0	360	360
c	Both-sided	50%	36	36	108
d	Both-sided	50%	36	54	126
e	One-sided	50%	36	36	108
f	One-sided	50%	36	54	126

Table 2 Description of models and results for reactions and strains

Model	Thinning type	Material	In-plane δ (mm)	Out-of-plane δ_y(mm)	ΔR (kN)	ε	$\Delta\varepsilon$
1	a	STS410	35	0	546	0.123	0.0187
2	b				180	0.152	0.0202
3	c				334	0.110	0.0223
4	d				314	0.099	0.0311
5	e				477	0.121	0.0172
6	f				409	0.099	0.0295
7	a	STS410	35	8.75	546	0.122	0.0187
8	b				180	0.148	0.0207
9	c				335	0.128	0.0310
10	d				318	0.114	0.0289
11	e				484	0.113	0.0214
12	f				417	0.116	0.0268
13	a	SS340	35	0	464	0.207	0.0236
14	b				147	0.288	0.021
15	c				275	0.234	0.0316
16	d				257	0.228	0.0326
17	e				410	0.179	0.0249
18	f				336	0.226	0.0312
19	a	STS410	35	17.5	546	0.122	0.0187
20	b				179	0.149	0.0199
21	c				334	0.137	0.0335
22	d				320	0.130	0.0213
23	e				486	0.094	0.0175
24	f				401	0.097	0.0286
25	a	STS410	50	0	584	0.141	0.0297
26	b				201	0.187	0.0295
27	c				362	0.098	0.0399
28	d				341	0.154	0.0514
29	e				521	0.108	0.0355
30	f				437	0.153	0.0483
31	a	STS410	20	0	424	0.019	0.0069
32	b				135	0.0467	0.0089
33	c				267	0.0367	0.0128
34	d				247	0.0410	0.0126
35	e				376	0.0269	0.0108
36	f				331	0.0384	0.0117

Six variations of the basic model were considered, as opposed to 23 variations in the earlier studies of Shiratori et al (2002), and Balan and Redekop (2005). The first of these variations, labelled model 'a', was an undamaged model, while the other five, labelled models 'b' to 'f', had various types of local thinning in the elbow. The five thinnings considered were respectively; fully circumferential (f.c.), both-sided with two levels of erosion, and one-sided with two levels of erosion. The latter four variations had been shown as critical in the two earlier studies. For the first level of erosion the total angle of erosion 't+2s' (Fig. 1) was 108^0, while for the second level of erosion the total angle was 126^0. The angle `s' represented the tapered part of the geometry in the meridional direction, while the angle 't' the maximum depth part. Fig.1 shows thinning on one side only, the two-sided thinning models had thinning on the right crown also. Tapering of the erosion in the longitudinal direction was limited to a maximum angle of 10^0 in the tapered part (Fig. 1). The maximum erosion in the current study was taken as 50% of the thickness. The full details of the thinning for the six distinct variations are given in Table 1. Analyses were carried out for the six variations for two different material properties, and for five different displacement-controlled loading conditions, forming six groups of models overall.

The materials considered were STS410 steel and SS304 steel. Both materials were taken as bilinear elasto-plastic with a kinematic hardening. In the elastic range the Young's modulus for both materials was taken as 210 GPa and the Poisson's ratio as 0.3. In the plastic range the yield stress and work hardening rates for the STS410 steel were taken respectively as 424 MPa and 500 MPa, while for the SS304 steel these constants were taken respectively as 344 MPa and 230 MPa. The material models are depicted in Figs. 2-3.

For all models studied an internal pressure of 9.8 MPa was assumed. The end of the right straight pipe was taken as fixed, while a displacement-controlled loading was applied to the end of the left straight pipe. A displacement-controlled cyclic separation of the ends of the straight sections of the piping elbow along a line joining the two ends (Fig. 4) was applied. The variations in the loadings considered concerned both the maximum prescribed displacement, and the direction of the displacement. Three bending cases labelled as 'in-plane' were defined with maximum displacements δ of 20, 35, and 50 mm along the line joining the centers of the ends. Two loading cases labelled as 'bi-directional' were defined, which had maximum in-plane displacements δ of 35 mm along the centers line, and simultaneous maximum displacement δ_y of either 8.75 mm or 17.5 mm in the perpendicular out-of-plane direction. The full description of the 36 models, with regard to thinning, material properties, and prescribed displacement loadings is given in Table 2.

The loading consisted of 33 cycles of prescribed displacements. In the first five cycles the amplitude of the displacement was gradually increased to its maximum value, whereas in the last five cycles it was gradually decreased to zero (Fig. 5). A total of 1160 steps decribed the cycles of the loading, with a typical increment per displacement step of 3mm. This general loading pattern was used for both the in-plane and bi-directional cases. For the bi-directional loading case the second displacement component was in-phase and simultaneous with the first component.

3. FINITE ELEMENT METHOD

The analysis was carried out using the ADINA 8.1 software run on a PC with a Pentium IV 2.8Hz processor. Shell elements were employed, since in an earlier study by Shiratori et al (2002) it had been demonstrated that a three-dimensional analysis was about 10 times as time-costly as a shell analysis, with an increase in accuracy of only about 8%. The analysis was quasistatic, with inertial effects being negligible in the time period considered. The FEM model for the nonlinear analysis was based on kinematic hardening, the associated flow theory, and the von Mises yield criterion. Shell elements with 4 nodes and 24 degrees of freedom were used. The typical model incorporated some 1400 elements. The fineness of the FEM mesh was similar to that of Shiratori et al (2002) and Balan and Redekop (2005), representing a limit of practical analysis with available tools.

Variations in the models studied included positioning of the thinned area, material properties, and magnitude and direction of the prescribed displacements in the loading. Six distint meshes were formulated, corresponding to the six distinct geometric models. There were minor differences in the six meshes, to accommodate the differences in the details of the thinning. In the circumferential direction generally 26 elements were taken. In the longitudinal direction following the pipe axis 10 elements were taken in each straight section and 18 in the elbow section. In the portions of the geometry where there was tapering of the thickness, 6 elements were taken in the longitudinal direction.

To model the displacement-controlled loading the center point of the end of the right straight pipe was fixed in all six degrees of freedom. At the center point of the end of the left straight pipe a displacement δ was prescribed. For the in-plane bending cases the displacement was in the plane of the center line of the pipe (XZ plane), along the line joining the two end points of the pipe (Fig. 4). For the bi-directional loading there was a

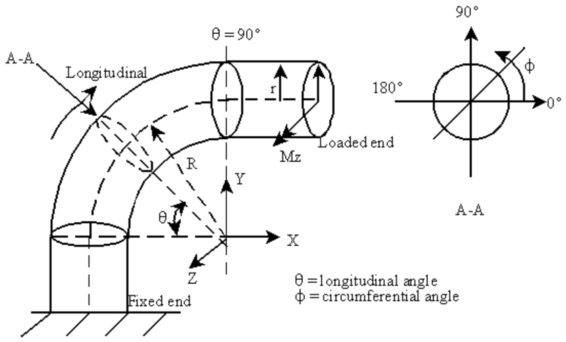

(a) Geometry

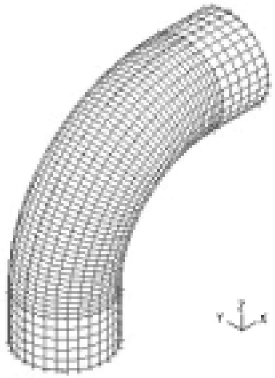

(b) FEM mesh

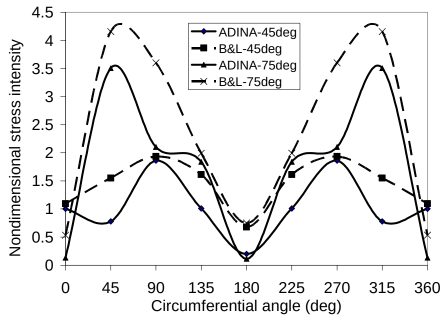

(c) Comparison – out-of-plane bending

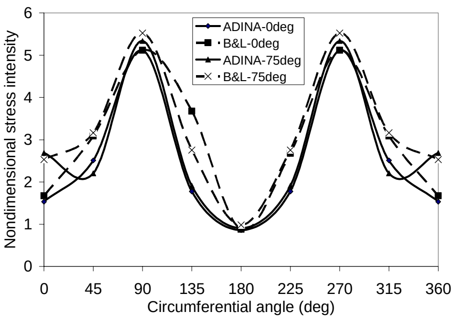

(d) Comparison – in-plane bending

Fig. 6 Validation 1

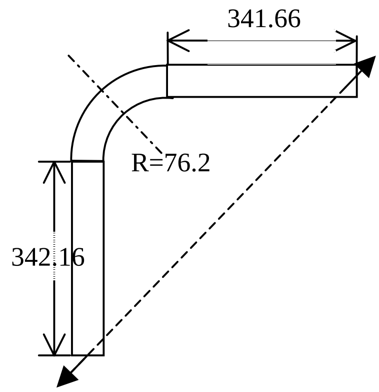

(a) Geometry

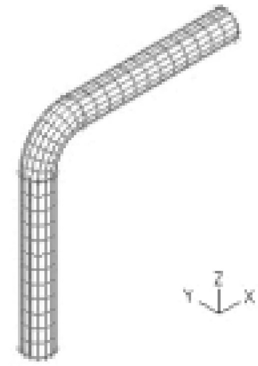

(b) FEM mesh

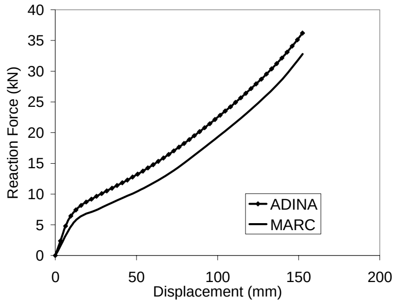

(c) Comparison – opening mode

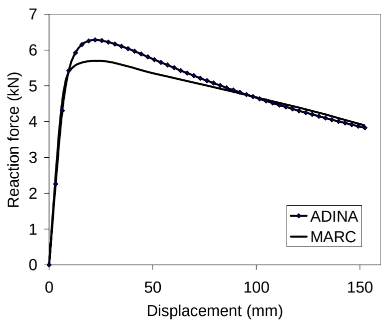

(d) Comparison – closing mode

Fig. 7 Validation 2

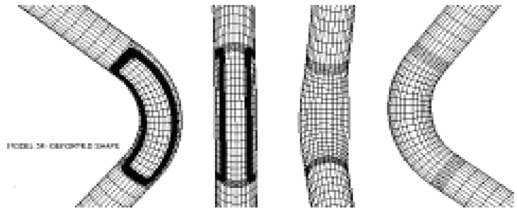

(a) Model 34

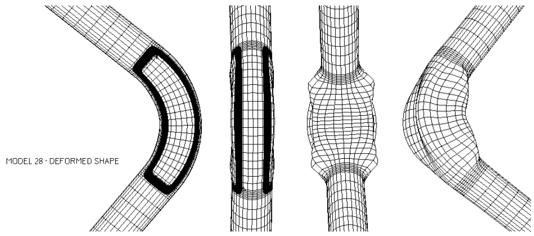

(b) Model 4

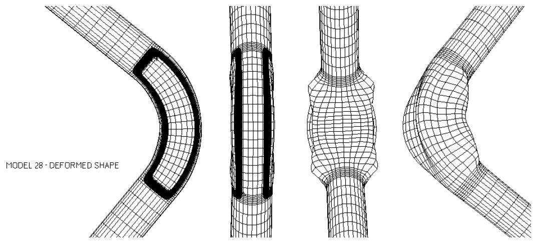

(c) Model 28

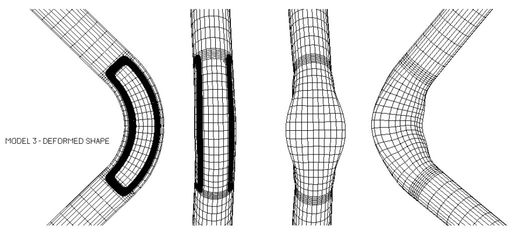

(d) Model 1

Fig. 8 Deformations – in-plane bending

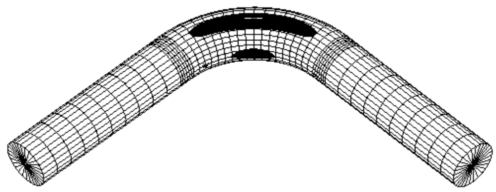

(a) Model 34

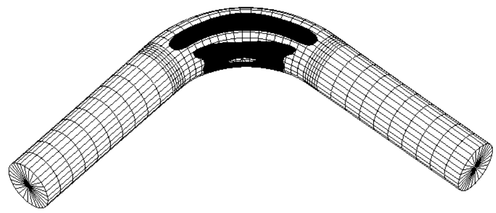

(b) Model 4

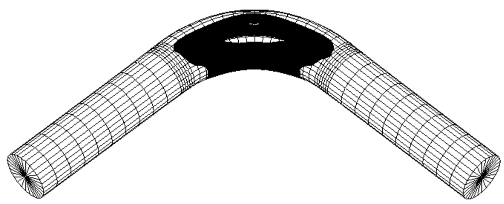

(c) Model 28

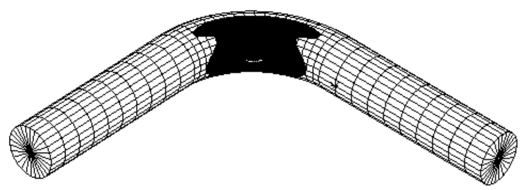

(d) Model 1

Fig. 9 Strain contours – in-plane bending simultaneous prescribed displacement δ_y at the left end in the Y direction. The principal output of the analysis was the set of displacements and strains in the pipe, and the reaction force at the left end.

4. VALIDATION

To obtain a perspective on the accuracy of the current approach two validation studies were conducted. The two studies concerned problems of linear and non-linear stress analysis of undamaged piping elbows, previously reported in the literature. The first of these problems (Basaraju and Lee, 1993) concerned the stress intensity in pressurized piping elbows subjected to out-of-plane and in-plane bending moments. The second of these problems (Tan and Matzen, 2002) concerned the determination of the elasto-plastic behavior of an undamaged piping elbow subject to in-plane opening and closing displacements.

The geometry and results for the first validation problem are shown in Fig. 6. The specific geometry studied was elbow 14B of Basaraju and Lee (1993). The elbow had a bend radius of 553 mm, a cross-sectional radius of 173 mm, and a wall thickness of 9.5 mm. The geometry and the FEM mesh of the current analysis are shown in parts (a) and (b) of the figure. Comparisons of results for the stress intensity for out-of-plane bending at two sections are given in part (c), while similar comparisons of results for in-plane bending are given in part (d). The two plots indicate that there is good agreement in the results between the previous and current study.

The geometry and results for the second validation problem are shown in Fig. 7. The piping elbow studied was a 900, 2'' schedule 10, long radius pipe, with seamless butt welding, with straight pipe segments about five times the outside diameter of the cross-section connected to each end. The material was SS304, which was defined as a multi-linear plastic material with stress-strain points as follows; (0.002, 265.0), (0.035, 344.73), (0.083, 413.68), (0.14, 482.63), (0.235, 551.58), (0.385, 568.81). Results were obtained by Tan and Matzen (2002) using the MARC FEM program for a prescribed displacement δ along the line of centers joining the ends. The geometry of the elbow is shown in part (a) of the figure and the FEM mesh of the current analysis in part (b). Comparisons of reaction-displacement plots for an opening mode controlled displacement are given in part (c) of the figure, while similar comparisons for the closing mode are given in part (d). The two comparisons indicate that there is good agreement between the previous and current study in both the elastic and plastic ranges.

5. RESULTS

A summary of the numerical results for the 36 models considered in this study is given in Table 2. The main results cited are range of reaction ΔR, final magnitude of hoop strain ε at the position of maximum strain concentration, and range of hoop strain $\Delta\varepsilon$ at this same position. Sample plots for deformation of models are given in Fig. 8, which also indicate the FEM mesh density. Sample hoop strain contour plots, hysteresis plots, and plots of strain histories are given in Figs. 9-13, while diagrams showing the effect of the magnitude and direction of the prescribed displacement on reaction range, strain magnitude, and strain amplitude are given in Figs. 14-15. The figures generally serve to exhibit the extreme cases of behavior of the various models.

5.1 Deformation plots

The plastic deformation occurred mainly in the intrados and crown parts of the elbow. Due to the local thinning the deformation plots for different models differed slightly. Within the six groups of models the f.c. thinning models had the most severe deformations. The patterns of deformation within the various groups showed strong similarity, due to the similarity in the respective thinning patterns.

The deformation plots for models 34, 4, 28 and 1 are shown in Fig. 8. These models were all subject to in-plane bending, and had the 'd' type of thinning (except model 1), with erosion on both sides. This thinning variation model had the worst cases in the various groups. The maximum prescribed displacement δ for models 34, 4, and 28 were respectively 20, 35, and 50 mm. It is seen from Fig. 8 that the plastic deformation took place mostly in the intrados part of the elbow. There was relatively little deformation in model 4, while there was large deformation in both models 4 and 28.

5.2 Strain contours

In the post-processing the location of the maximum hoop strain was identified for each model, and then a study was made of the hoop strain magnitude and amplitude. Nodes in the elbow of the structure typically had the largest strains. The results for the strains are tabulated in Table 2. The group experiencing the largest strains was the one for the SS340 material, with in-plane prescribed displacement of 35 mm. The group experiencing the lowest strain level was the SS410 one, with an in-plane displacement of 20 mm. Concerning strain amplitude, the models of the group subjected to 50 mm prescribed displacement experienced the largest values.

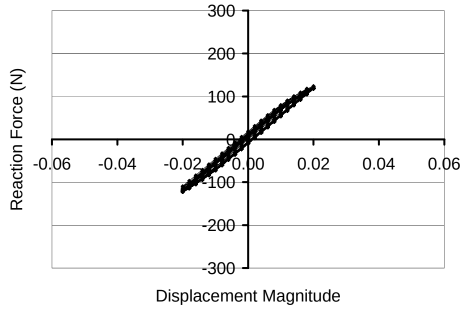

(a) Model 34

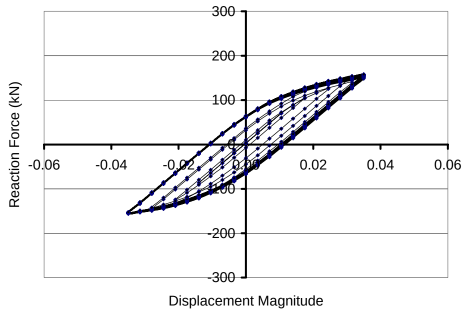

(b) Model 4

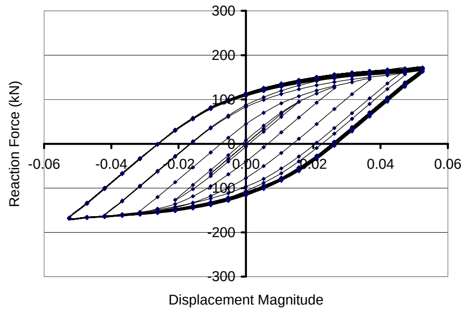

(c) Model 28

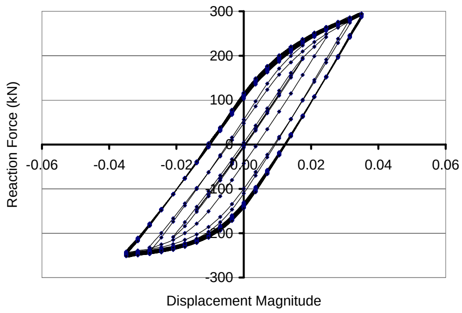

(d) Model 1

Fig. 10 Hysteresis plots – in-plane bending

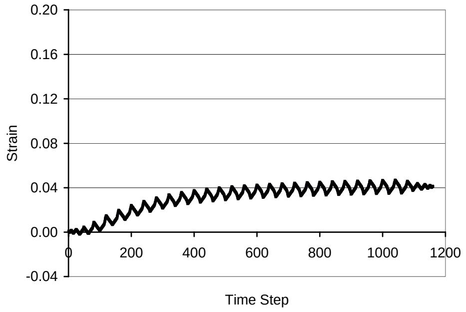

(a) Model 34

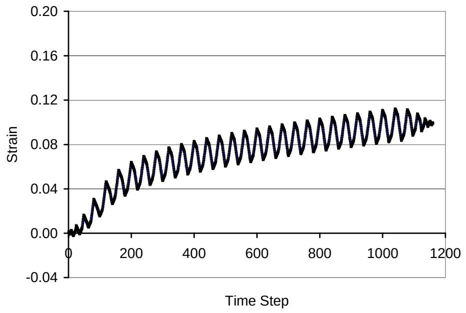

(b) Model 4

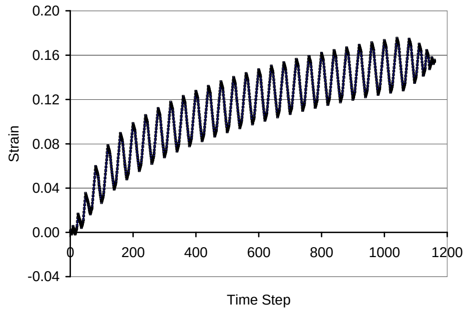

(c) Model 28

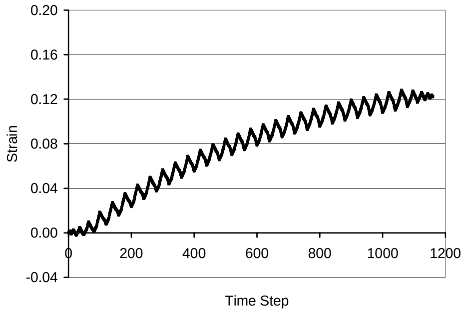

(d) Model 1

Fig. 11 Strain histories – in-plane bending

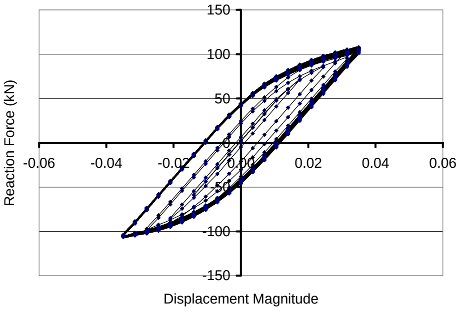

(a) Model 4

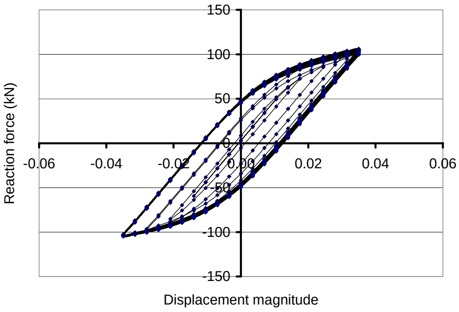

(b) Model 10

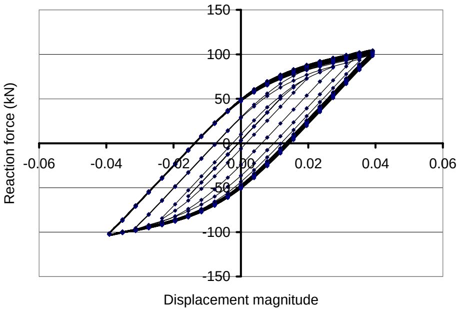

(c) Model 22

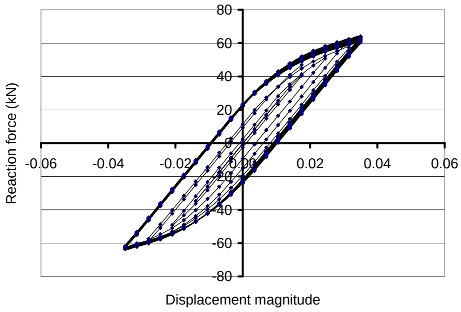

(d) Model 2

Fig.12: Hysteresis plots – bi-directional bending

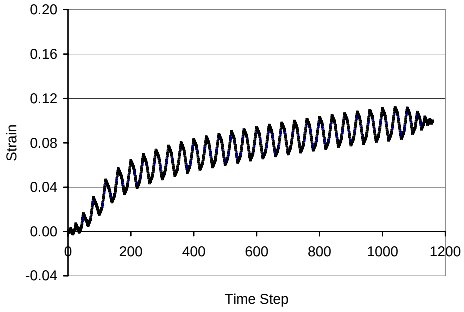

(a) Model 4

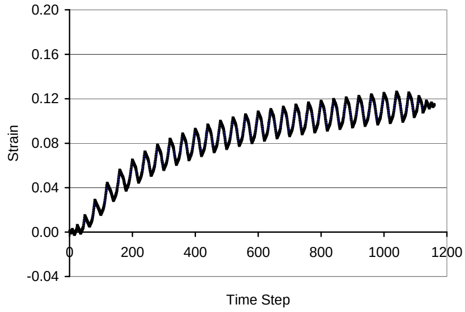

(b) Model 10

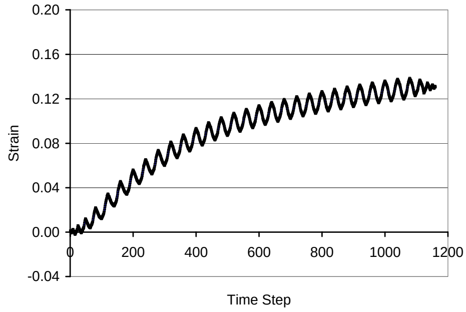

(c) Model 22

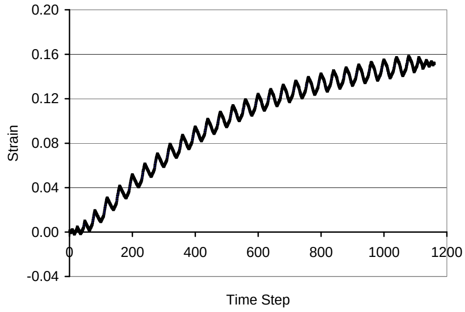

(d) Model 2

Fig. 13: Strain histories – bi-directional bending

The strain contour plots for models 34, 4, 28 and 1 are shown in Fig. 9. These are the models with both-sided thinning also represented in Fig. 8. An increase of the darkness of the shade indicates an increase of the strain level. It is evident from Fig 9 that the strain pattern was very similar in the various models, but the magnitudes of the strain increased in the sequence of models 34 to 4 to 28. There was relatively large deformation in model 1, which was subject to the large prescribed displacement δ of 35 mm.

5.3 Hysteresis plots and strain histories for in-plane bending

The hysteresis plots represent the variation of the end reaction with the prescribed displacement, which passes through the cycle defined by Fig. 5. For in-plane loading two reaction components were found from the FEM results, while for the bi-directional loading three components were found. Resultants were found from the components. The values cited herein excluded the reaction stemming from the internal pressure. The strain history plots represent the variation of the magnitude of the hoop strain with time step at the position of maximum strain in the piping elbow. These latter diagrams give information about both the magnitude and range of the strain as the elbow is subjected to the cyclic displacement.

The hysteresis plots of Fig. 10, given for models 34, 4, 28 and 1, are for the in-plane bending case. These are the same models that were represented in Figs. 8 and 9. In part (a) of the figure it is seen that for the lowest prescribed displacement case there was essentially elastic behavior. In part (c) of the figure it is seen that for the highest prescribed displacement case there was extensive plasticity. The undamaged model 1, subjected to the intermediate prescribed displacement, also experienced a modest level of plasticity. The strain histories of Fig. 11 for these same models indicate similar behavior.

5.4 Hysteresis plots and strain histories for bi-directional bending

The hysteresis plots of Fig. 11, given for models 4, 10, 22 and 2, are for the bi-directional bending case. These models again had the ‘d’ type of thinning (except model 2) but were subjected to bi-directional bending. In parts (a-c) of the figure it is seen that there was relatively little change in the hysteresis diagrams, as the maximum out-of-plane prescribed displacement δ_y was increased from 8.75 to 17.5 mm. The diagram for the undamaged model 2 in part (d) of the figure indicates relatively low reaction force and plasticity. The strain histories of Fig. 13 for these same models indicate similar behavior.

5.5 Effect of magnitude of prescribed displacement on reaction, strain magnitude and amplitude

The effect of the magnitude of the prescribed displacement for in-plane and bi-directional bending on the response is shown in Figs. 14 and 15 respectively. Three responses were considered for each of the two loading cases, namely reaction range, strain magnitude, and strain amplitude. For the in-plane bending results of Fig. 14 three levels of displacement δ are represented, namely 20, 35 and 50 mm For the bi-directional bending results of Fig. 15 three levels of out-of-plane displacement δ_y, 0, 8.75, 17.5 mm (coupled with a simultaneous in-plane displacement of 35 mm) are represented. In each figure models having wall details of the type ‘a’, ‘b’, ‘c’, ‘d’, ‘e’, and ‘f’ of Table 1 are given.

In five of the six parts of Figs. 14-15 it is seen that the model that experienced the maximum effect at the lowest prescribed displacement also experienced the maximum effect at the intermediate and maximum prescribed displacement. The exception was the plot for the strain amplitude for the bi-directional loading. The model experiencing the maximum reaction, as well as the maximum strain magnitude, for both types of loading was type ‘a’. The model experiencing the maximum strain amplitude for in-plane bending was model ‘f’. For bi-directional bending model ‘e’ experienced the maximum strain amplitude at the lowest prescribed displacement, while model ‘f’ experienced the maximum strain amplitude at the intermediate and highest prescribed displacements.

5.6 Miscellaneous observations

Two materials were considered for the piping elbows, namely STS410 and SS340. The results indicated that the STS410 models experienced greater plastic deformation, thus absorbing greater amounts of energy. The respective reaction ranges were 546 kN and 464 kN for the uneroded models. The level of out-of plane displacement considered in the study was relatively low, and did not lead to significant increases in the plasticity of the models. Models identified as having large fatigue parameters in the current study were generally also identified in this way in the earlier studies of Shiratori et al (2002), and by Balan and Redekop (2005).

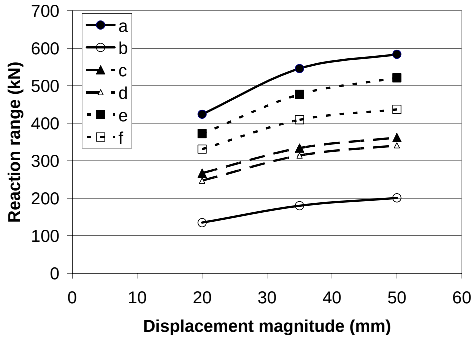

(a) Reaction range ΔR

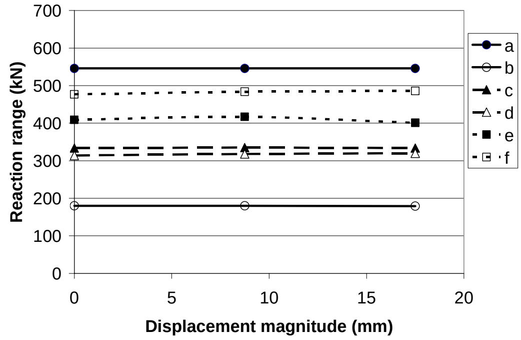

(a) Reaction range ΔR

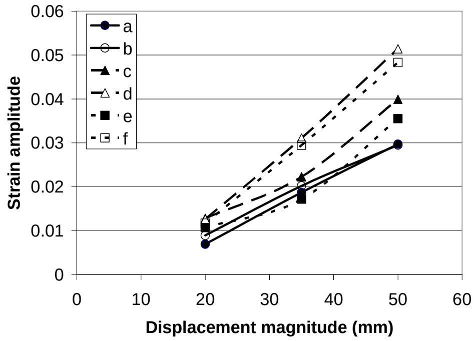

(b) Strain magnitude ε

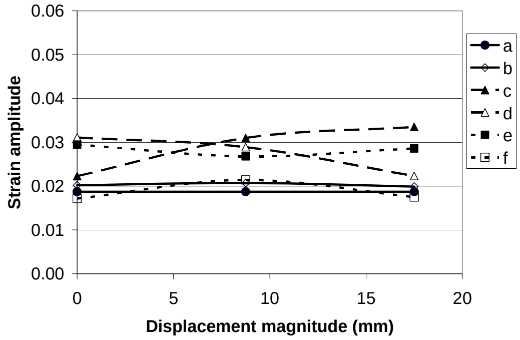

(b) Strain magnitude ε

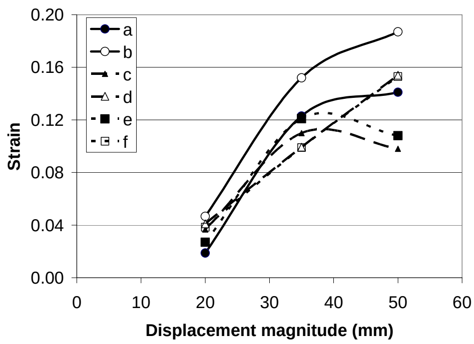

(c) Strain amplitude Δε

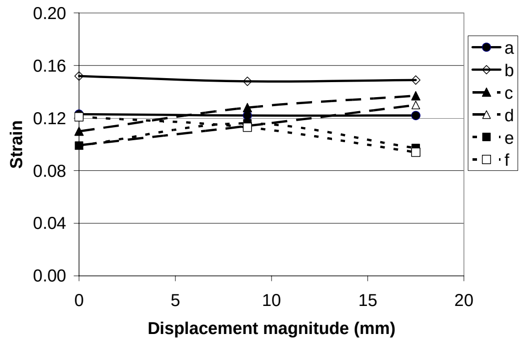

(c) Strain amplitude Δε

Fig. 14 Effect of magnitude of δ on in-plane bending results

Fig. 15 Effect of magnitude of δ_y on bi-directional bending results

6. CONCLUSIONS

The effect of local thinned areas on the fatigue characteristics of piping elbows has been studied. Including out-of-plane prescribed displacements did not lead to a major increase in the fatigue parameters relative to the in-plane results. The thinning model experiencing the maximum effect at a low prescribed displacement level generally also had the maximum effect at other displacement levels. In comparing the response of the two materials studied it was observed that the STS410 steel experienced the higher plastic deformations. The current results are available for qualitative fatigue assessment of elbows using existing fatigue theories.

REFERENCES

Balan, C., Redekop, D., (2005), Int. J. Press. Ves. Piping, Vol. 82, No. 3, pp. 235-242.

Basaraju, C., Lee, R.L., (1993), ASME PVP-244, pp. 102-112.

Kulkarni, S.C., Kant, T., Reddy, G.R., Prasa, P., Vaze, K.K., Gupta, C., (2004), Int. J. Press. Ves. Piping, Vol. 81, pp. 609-617.

Miyazaki, K., Nebu, A., Ishiwata, M., Hasegawa, K., (2002), Nucl. Eng. Design, Vol. 214, pp. 127-136.

Mourad, H.M., Younan, M.Y.A., (2001), J. Press. Ves. Tech., Vol. 123, pp. 253-2001.

Mukaimachi, N., Ando, F., Ikeda, M., (2002), ASME PVP-445-1, pp. 119-126.

Nakamura, I., Otani, A., Shiratori, M., (2004), J. Press. Ves. Tech., Vol. 126, pp. 85-90.

Robertson, A., Li, H.J., Mackenzie, D., (2005), Int. J. Press. Ves. Piping, Vol. 82, pp. 407-416.

Shim, D.J., Choi, J.B., Kim, Y.J., Kim, J.W., Park, J.Y., (2002), ASME PVP-442, pp. 125-130.

Shiratori, M., Ochi, Y, Nakamura, I., Otani, A., (2002), ASME PVP - 445(1), pp. 7-16.

Tan, Y., Matzen, V., (2002), Nucl. Eng. Des., Vol. 217, pp. 21-39.

Weisz, E., Lietzmann, A., Rudolph, J., (1996), Int. J. Press. Ves. Piping, Vol 671, pp. 211-217.

Zhang Li, Wang Yinpei, Chen Jin, Liu Cengdian, (2001), Int. J. Press. Ves. Piping, Vol. 78, pp. 697-703.

